Generation of Dark and Bright Spin Wave Envelope Soliton Trains through Self-Modulational Instability in Magnetic Films

Mingzhong Wu,[1] Boris A. Kalinikos,[2] and Carl E. Patton[1]
[1]*Department of Physics, Colorado State University, Fort Collins, Colorado 80523, USA*
[2]*St.Petersburg Electrotechnical University, 197376, St.Petersburg, Russia*
(Received 18 June 2004; published 7 October 2004)

The generation of dark spin wave envelope soliton trains from a continuous wave input signal due to spontaneous modulational instability has been observed for the first time. The dark soliton trains were formed from high dispersion dipole-exchange spin waves propagated in a thin yttrium iron garnet film with pinned surface spins at frequencies situated near the dipole gaps in the dipole-exchange spin wave spectrum. Dark and bright soliton trains were generated for one and the same film through placement of the input carrier frequency in regions of negative and positive dispersion, respectively. Two unreported effects in soliton dynamics, hysteresis and period doubling, were also observed.

DOI: 10.1103/PhysRevLett.93.157207 PACS numbers: 75.30.Ds, 76.50.+g, 85.70.Ge

Two types of envelope solitons, bright and dark, can propagate in nonlinear dispersive media. The main control factors are (1) the curvature of the dispersion characteristic and (2) the change in the carrier frequency with signal amplitude. When the signs of the parameters that represent these factors are opposite, one has an attractive nonlinearity and one can form bright solitons. When the signs are the same, one has a repulsive nonlinearity and dark solitons are possible [1,2]. There are also two main approaches to the generation of such solitons: (1) the excitation of individual solitons through an application of appropriate input pulses and (2) the formation of envelope soliton trains from large amplitude continuous wave (cw) input signals. For (2), the periodic soliton pulse sequences are formed through (a) self-modulational instability (SMI) process in the case of a single cw input signal or (b) induced modulational instability process in the case of two cw input signals.

As is well known, the modulational instability for nonlinear waves can be studied in two domains, the frequency domain and the time domain [1,3]. If the modulational instability as evolved from a cw signal is well developed, one will observe a comb of frequency harmonics in the frequency domain and a train of nonlinear pulses in the time domain. Although not recognized as solitons at the time, even the pivotal work on nonlinear waves by Fermi, Pasta, and Ulam [4] considered modulational instability processes in which a nonlinear continuous wave breaks into a periodic train of localized nonlinear wave packets, e.g., bright solitons.

Through the induced modulational instability process as well as through pulse excitation, both the formation of bright solitons for waves with attractive nonlinearity and dark solitons for waves with repulsive nonlinearity have been observed in a variety of physical systems, such as water, plasmas, optical fibers, electrical transmission lines, and magnetic thin films [1,3]. Through the SMI process, the formations of bright solitons from waves with attractive nonlinearity have also been observed. Examples include optical solitons [5], electrical transmission line solitons [6], and spin wave soliton trains [7].

However, no dark solitons have ever been produced through an SMI process. This Letter reports first results on the SMI production of dark solitons. The new results go even further. The dipole gaps in the spin wave spectrum of a thin yttrium iron garnet (YIG) film was used to achieve both attractive and repulsive nonlinearity conditions for one and the same propagation configuration. Through a simple change in frequency from one side of the dipole gap to the other, it is possible to produce bright and dark solitons. The solitons were in the form of trains. The SMI formation process also shows two previously unreported effects in soliton dynamics, hysteresis and period doubling.

The experiments used a long and narrow 5.4 μm thick single-crystal YIG film strip in a microstrip transducer structure [8]. The strip was cut from a large area liquid phase epitaxy film. The input and output microstrip transducers were positioned along and just above the film strip, with a transducer separation of 9 mm. An in-plane static magnetic field of 1074 Oe was applied perpendicular to the long direction of the strip.

The orthogonal in-plane field/propagation direction configuration corresponds to the magnetostatic surface wave (MSSW) configuration. The in-plane field geometry results in a negative nonlinear frequency response parameter N, taken as $\partial\omega_k/\partial|u|^2$, where ω_k is the spin wave frequency, and $u = m/2^{1/2}M_s$ defines a reduced dynamic response amplitude in terms of the transverse rms dynamic magnetization m and the saturation magnetization M_s. This negative N parameter, in combination with the dispersion parameter $D = \partial^2\omega_k/\partial k^2$, where k is

 0031-9007/04/93(15)/157207(4)$22.50

the wave number, serves to define the nonlinearity as attractive ($ND < 0$) or repulsive ($ND > 0$).

The film had pinned surface spins, and the corresponding dipole-exchange spin wave dispersion characteristic exhibited a regular series of dipole gaps [9]. A shift in the operating point frequency from one side of a given gap to the other allows one to change from an $\omega_k(k)$ response with positive curvature and $D > 0$, and an attractive nonlinearity, to one with negative curvature and $D < 0$, and a repulsive nonlinearity. This ability to shift from one side of the dipole gap to the other is the key control parameter for the new results reported below.

Detailed measurements of the power dependent transmission versus frequency (TvF) response profiles for the structure preceded the soliton experiments. As in previous work [9,10], the TvF profiles at low power yielded the dispersion characteristics of the film, the MSSW lower band edge cutoff frequency, and the frequency positions of the dipole gaps. The MSSW lower cutoff frequency was about 4988 MHz. As the power was increased, the passband was found to shift to lower frequency, as expected for the MSSW configuration and a negative N parameter. Depending on the input power levels, frequency down-shifts as large as 25 MHz were observed.

The power dependent TvF profile determinations were then used as a basis for the high power cw SMI experiments. Input cw signals were applied for a range of frequency f_{in} values on both sides of selected dipole gaps and over a range of cw input power P_{in} levels from 25–34 dBm. For each combination, both power versus time profiles and power-frequency spectra were obtained. Keep in mind that the curvature of the $\omega_k(k)$ dispersion response and, therefore, the dispersion parameter D as well, changes sign as one moves across a dipole gap.

Figure 1 shows the key results for dark soliton train formation, hysteresis and period doubling. The top panel [Fig. 1(a)] shows the TvF profile in the vicinity of dipole gap number 5 in the MSSW dipole-exchange spin wave spectra for this film, along with the indicated $f_{\text{in}} = 4979.0$ MHz operating point just below the gap point at $f_g = 4979.3$ MHz, as indicated. The TvF profile was recorded by sweeping the frequency at $P_{\text{in}} = 25.1$ dBm. The indicated f_{in} operating point was used for all of the data in the lower panels in the figure. For $f_{\text{in}} < f_g$, one has $D < 0$ and the repulsive nonlinearity condition that matches dark soliton production. The left and right graphs in graph sets (b) through (f) of Fig. 1 show the output power versus time (PvT) profiles and the corresponding power versus frequency (PvF) spectra specific to the time responses, respectively, for a sequence of P_{in} levels as shown. For (b) through (d) of Fig. 1, P_{in} is stepped up in 0.1 dB steps from 25.1 dBm, while for (d) through (f), P_{in} is then stepped back down to the starting point in 0.1 dB steps. As will become clear from the discussion below, the kind of step-up and step-down sequence shown in Fig. 1 is critical to the realization of dark solitons by the SMI process.

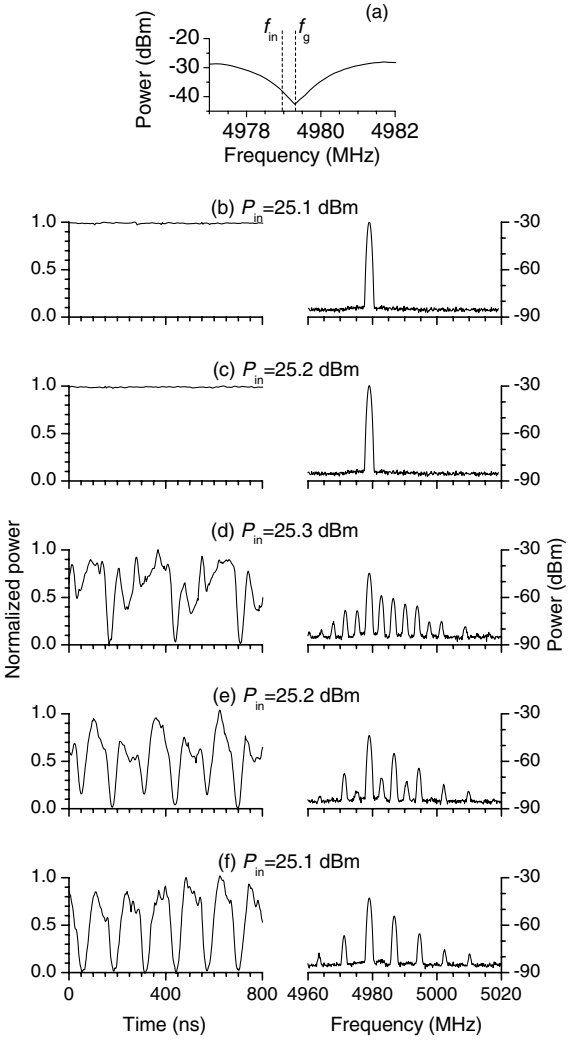

FIG. 1. Representative SMI results for repulsive nonlinearity. Graph (a) shows the transmission versus frequency profile for a YIG film delay line structure, with the operating frequency f_{in} as indicated. Graphs (b)–(f) show output power versus time profiles and power-frequency spectra for a sequence of increasing and then decreasing input power P_{in} levels, as indicated.

As shown in graphs (b) and (c) of Fig. 1, one observes no modulational instability when the input power is initially stepped up from 25.1 to 25.2 dBm. Graph (d), however, shows that the second step-up in power to $P_{\text{in}} = 25.3$ dBm causes an abrupt change in the response. Here, the PvT profile appears as a somewhat distorted dark solitonlike train, and the PvF spectrum shows multiple peaks with a uniform frequency comb character. The $P_{\text{in}} = 25.3$ dBm power point may be termed an onset threshold.

The step-down results in (e) and (f) of Figure 1 are even more interesting. These data show that the overall step-up/step-down response is not reversible. After the first step down to 25.2 dBm, as in (e) of Fig. 1, the gray

dips in the previous PvT profiles become stronger and alternate peaks in the PvF profile drop in intensity. After the second step down to 25.1 dBm, as in Fig. 1(f), the period of the dark soliton train is reduced by a factor of 2, relative to the train in (d) of Fig. 1, the frequency comb cleans up completely, and the PvF peak spacing has doubled. For a further reduction in power below 25.1 dBm, the PvT and PvF profiles revert back to the original low power form as in Fig. 1(a). The $P_{\text{in}} = 25.1$ dBm power point may be termed a dropout threshold.

Three important new results are evident from Fig. 1. (1) The data demonstrate the first generation of dark solitons through the SMI process. The dips in the PvT profiles in Figs. 1(d) and 1(f) go essentially to zero, so that the soliton trains are actually black soliton trains. (2) The instability data are hysteretic. That is, the data show two distinct thresholds. The SMI onset threshold point, when the input power is initially increased from some low level in the linear regime, is actually higher than the dropout threshold power needed to maintain an SMI response if the power is later decreased. (3) The instability hysteresis response is accompanied by a soliton train period-doubling or period-halving effect. As the power is decreased from the initial SMI onset point, as in (d) of Fig. 1, to the SMI dropout point, as in (f) of Fig. 1, there is a soliton train period halving. If the power is then increased back to the initial onset threshold, the process is reversible. Intuitively, the period-doubling phenomena may be expected as a typical initial route to chaos in nonlinear systems [11].

Figure 2 shows parallel results for an attractive nonlinearity condition and bright soliton generation. The data are for an operating point at $f_{\text{in}} = 4979.6$ MHz. This f_{in} value corresponds to a frequency point to the right of the f_g gap point in Fig. 1. For $f_{\text{in}} > f_g$, one has $D > 0$ and the repulsive nonlinearity that matches bright soliton generation. The format of the three sets of graphs follows the format in Fig. 1. The graphs show PvT and PvF profiles for a sequence of three P_{in} levels that start at the initial onset threshold of 25.3 dBm and end at the dropout threshold of 25.1 dBm. For brevity, the initial linear response profiles that correspond to the (b) and (c) graph sets in Fig. 1 are not shown. Note that the onset and dropout thresholds are identical to those for the dark soliton data in Fig. 1. The data were obtained in the same way as those in Fig. 1, by starting at a P_{in} value well below the dropout threshold and increasing the cw power in small steps.

The data in Fig. 2 show the same type of responses shown in Fig. 1, except that operation in the attractive nonlinearity regime now leads to bright solitons. The pulse trains now have the PvT profiles expected for bright solitons, in the form of steep and narrow pulses. The PvF profiles for these pulses consist of a uniform comb structure. The data show the same period-doubling response as

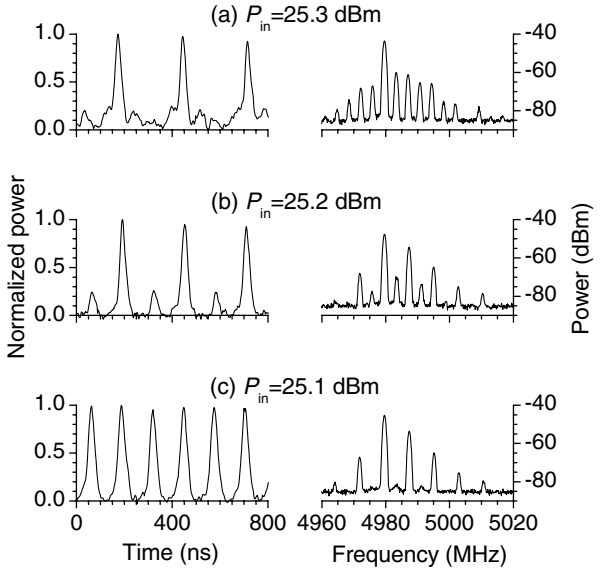

FIG. 2. Representative output power-time profiles and power-frequency spectra for different input power P_{in} levels, which were stepped down in 0.1 dBm steps from 25.3 dBm as indicated. The operating point $f_{\text{in}} = 4979.6$ MHz is above the gap point f_g.

well. The soliton period in Fig. 2(c) is one half the period in Fig. 2(a), with corresponding changes in the frequency spacing for the PvF profiles.

There are two additional points of note for the data in Fig. 2. First, note the zero background level for the bright pulse trains. This point is important because the bright solitons that are excited through SMI processes in other media, such as deep water or electrical transmission lines, for example, typically have a nonzero background level [1,6]. Second, note that the soliton pulse width does not change during the period halving or period doubling that is produced by the change in power. This point is important because it shows that one can control the soliton period without affecting the width of the individual pulses.

In addition to the soliton train profiles shown in Figs. 1 and 2 , additional data were obtained as the operating point frequency f_{in} was moved from the below gap to the above gap condition. This frequency shift gave a systematic change in the train response. For an operating point frequency well below f_g, and to the left of the f_{in} value shown in Fig. 1, one finds dark solitons with dips that do not go all the way to zero power. Such pulses are usually called ''gray'' solitons. As the operating point is then moved toward the gap frequency from below, one obtains the completely black soliton profiles shown in Fig. 1. As f_{in} approaches f_g, the background level becomes smaller and smaller and the pulse structure becomes indiscernible. As f_{in} is increased further and moves above the gap point, a bright pulse train response against a zero background, as shown in Fig. 2, is realized. Further increases

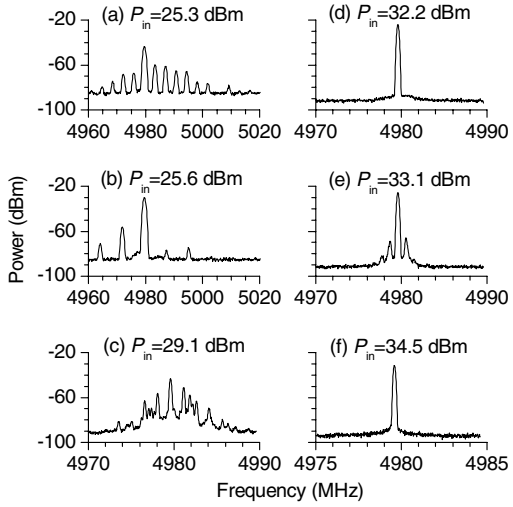

FIG. 3. Representative output power-frequency spectra for different input power P_{in} levels, as indicated. The frequency operating point was at $f_{in} = 4979.6$ MHz, the same as for the data of Fig. 2.

in the frequency to well above f_g then cause the background level to increase.

The new SMI soliton train results in Figs. 1 and 2 occur for relatively small changes in power. There are important additional changes in these responses if the power is increased above the onset threshold. Example results are shown in Fig. 3. These data are for $f_{in} = 4979.6$ MHz, the same as for the above gap Fig. 2 data. The same effects were found for below gap conditions as well. The figure shows six PvF profiles, starting from the initial $P_{in} =$ 25.3 dBm onset power point shown in graph (a) of Fig. 2 and increasing to the maximum available power of 34.5 dBm, as indicated. Note the frequency scale changes from graph to graph, and the changes in the instrument limited widths of the individual peaks.

These data show a number of changes in the PvF profile with power. First, there is an initial period-halving response, as in Fig. 3(b). This is followed by the formation of an irregular comb profile, a frequency compression of the overall spectrum, and then a narrowing to a single peak, as in Fig. 3(d). Further increases in power, as in (e) and (f) of Fig. 3 , lead to recurrence. Similar trends have been reported in [9,12], but the Fig. 3 data provide the first complete picture of a high power response that includes a period change, frequency compression, a route to chaos, and recurrence. Recurrence in an SMI process has not been reported previously. Note that the PvT soliton train profile that accompanies the PvF data in Fig. 3(a), also changes substantially with the increase in power. One finds, for example, a chaotic temporal response accompanies the PvF profile in Fig. 3(c) for the response power, and a level cw response for Figs. 3(d) and 3(f).

As of yet, there has been no theoretical modeling to deal with these new effects. Such analyses could be done in the framework of the nonlinear Schrödinger equation with higher order terms included or the Ginzburg-Landau equation.

In summary, this Letter reports the first experimental observation of the generation of dark solitons through self-modulational instability. The data show that it is possible to move from gray to black to bright soliton trains by moving the operating point frequency across a selected dipole gap in the dipole-exchange spin wave mode dispersion response. The soliton response is inherently hysteretic, with two power thresholds, one for onset and a slightly lower dropout threshold, as well as period halving or period doubling effects in the corresponding power versus frequency (PvF) spectrum. Higher powers lead to further changes in the power-frequency spectra, such as comb compression, chaos, and recurrence.

This work was supported in part by the National Science Foundation, Grant No. DMR-0108797; the U. S. Army Research Office, Grant No. DAAD19-02-1-0197; the North Atlantic Treaty Organization, Grant No. PST/CLG 980077; and the Russian Foundation for Basic Research, Grant No. 02-02-16485.

[1] M. Remoissenet, *Waves Called Solitons: Concepts and Experiments* (Springer-Verlag, Berlin, 1999).
[2] C. Sulem and P. L. Sulem, *The Nonlinear Schrödinger Equation: Self-Focusing and Wave Collapse* (Springer-Verlag, New York, 1999).
[3] Y. S. Kivshar and G. P. Agrawal, *Optical Solitons* (Academic, San Diego, 2003).
[4] E. Fermi, J. Pasta, and S. Ulam, Los Alamos Scientific Laboratory, Report No. LA-1940, 1955 (unpublished).
[5] K. Tai, A. Hasegawa, and A. Tomita, Phys. Rev. Lett. **56**, 135 (1986).
[6] P. Marquie, J. M. Bilbault, and M. Remoissenet, Phys. Rev. E **49**, 828 (1994).
[7] B. A. Kalinikos, N. G. Kovshikov, and A. N. Slavin, Pis'ma Zh. Tekh. Fiz. **10**, 936 (1984) [Sov. Tech. Phys. Lett. **10**, 392 (1984)].
[8] M. Chen, M. A. Tsankov, J. M. Nash, and C. E. Patton, Phys. Rev. B **49**, 12 773 (1994).
[9] B. A. Kalinikos, N. G. Kovshikov, and A. N. Slavin, Zh. Eksp. Teor. Fiz. **94**, 159 (1988) [Sov. Phys. JETP **67**, 303 (1988)].
[10] B. A. Kalinikos, N. G. Kovshikov, and A. N. Slavin, J. Appl. Phys. **67**, 5633 (1990).
[11] H. G. Schuster, *Deterministic Chaos: An Introduction* (John Wiley & Sons, New York, 1995).
[12] A. Prabhakar and D. D. Stancil, J. Appl. Phys. **79**, 5374 (1996).